Reagentless redox capacitive assaying of CRP at a polyaniline interface

Ausra Baradoke, Robert Hein, Xiaoxiong Li, Jason J. Davis*

Department of Chemistry, University of Oxford, South Parks Road, Oxford OX1 3QZ, U.K.

ABSTRACT: Methods that enable the sensitive and label-free detection of protein biomarkers are well placed to make potentially significant contributions to diagnostics and derived personalized healthcare. In supporting this goal a myriad of (electrochemical) methodologies have been developed; recently electrochemical capacitance spectroscopy (ECS) emerged as an impedance-derived approach which, in employing surface-confined redox-transducers, circumvents problems associated with the use of solution-phase redox-probes. Herein, we expand this scope by utilizing phytic acid-doped polyaniline (PANI-Pa) as a novel redox-charging polymer support enabling the reagentless assaying of C-reactive protein (CRP) in serum with good sensitivity. The construction of the sensory interface via electropolymerisation allows facile tuning of the polymers´ surface coverage and redox (capacitive) properties which in turn modulate both assay selectivity, fouling and sensitivity. Significantly, this methodology is readily extendable to a wide range of electrode materials and analytes.

The label-free detection of disease-specific biomarkers has potentially profound potential in diagnostics and point-of-care settings if performance is retained when scaled.[1–3] Electrochemical immunosensors are particularly promising sensory platforms, offering high sensitivity, rapid analysis, viable scalability, native multiplexing capability, and a low cost of fabrication.[4–7] As an inherently spectroscopic, highly sensitive analytical platform electrochemical impedance spectroscopy (EIS) has been increasingly employed for the label free analysis of a myriad of biomarkers, most commonly in a format where in the presence of a solution-phase redox probe the interfacial charge transfer resistance (R_{ct}) of a receptor-modified electrode is utilized as a signal transducer.[8–11] The need to dope any analytical solution with a very large excess of highly charged reagent is untidy and can be associated with deleterious effects. Some prior work has noted these challenges, where signal increase can be caused by either protein binding or baseline drift.[12–14] We have developed reagentless, capacitive approaches to EIS, most notably the use of surface-confined redox-transducers enabling sensitive signal transduction *via* a redox-capacitance (C_r).[15–17] The inherently high sensitivity of C_r on its local (dielectric) environment has been exploited in a variety of biosensors, whereby, almost exclusively, ferrocene (Fc) is utilized as a redox transducer.[18] The use of Fc, most commonly in self-assembled monolayers (SAMs) on gold, is however associated with certain drawbacks, particularly an often compromised redox and thus voltammetric/capacitative baseline stability.[19,20] Redox-active conducting polymers are promising candidates in such sensory interfaces, which due to their high tuneability (film thickness, monomer nature, doping state etc.) and ease of preparation (electropolymerisation on various conducting substrates) have been applied in numerous sensors.[21–26] As a result of their polymeric, 3-dimensional structure they are furthermore supportive of a high level of bioreceptor loading (relevant to sensor sensitivity).

In order to extend the scope of label-free capacitive sensors we have herein systematically investigated the redox capacitive properties of electropolymerised polyaniline (PANI) films. As a proof-of-principle we have utilized this platform in supporting the assaying of CRP in 1% of serum across its clinically relevant range.

EXPERIMENTAL

Electrochemical experiments: All electrochemical experiments were carried out with a PalmSens potentiostat in a three-electrode configuration comprising a screen-printed graphene nanoplate working electrode (SPE), a screen printed Ag reference electrode and a screen printed Au counter electrode. All potentials are reported with respect to the Ag reference electrode. All experiments were carried out in 0.1 M phosphate buffer (PB), pH = 7.4, unless otherwise stated. Cyclic voltammetry (CV) was carried out at a scan rate of 100 mV/s. Square-wave voltammograms (SWV) were measured with a step potential of 5 mV, an amplitude of 50 mV and a frequency of 10 Hz. Electrochemical impedance spectroscopy was performed between 9 kHz to 0.1 Hz (20 frequencies), with a sigmoidal AC perturbation of 10 mV (peak-to-peak). These experiments were carried out at different DC potentials including the "redox-in" potential (OCP; -0.16 V, the half-wave potential of PANI-film), the "redox-out" potential (0.4 V, no redox-activity) as well as between -0.8 – 0.4 V (20 mV potential steps) at a fixed frequency of 0.1 Hz with waiting time of 5 s. Impedance-derived capacitance was obtained via $C''(\omega) = Z'/\omega Z^2$ and $C'(\omega) = Z''/\omega Z^2$, where ω is the angular frequency. The capacitance of the interface was obtained either graphically as the diameter of the semicircular region in the capacitive Nyquist plots of via circuit fitting as discussed in the main text. Circuit fitting and data analysis was carried out with PSTrace software 5.7. The relative response (RR%), i.e. the decrease in C_r, was normalised as follows: $RR\% = -\frac{C_r - C_{r_0}}{C_{r_0}} * 100\%$. Langmuir-Freundlich isotherms were fitted according to $\theta = \frac{K*[CRP]^n}{1+K*[CRP]^n}$. The limit of detection (LOD) was determined according to

$LOD = \frac{3*\sigma}{s}$, where s is the slope of the linear region of the calibration curve and σ the standard deviation of the blank.

Sensor construction: The electrodes were washed with copious amounts of water followed by electrochemical polishing in 0.1 M KOH, between -1.0 to 1.3 V for 20 cycles. The electroactive surface area of the cleaned electrodes was determined via the Randles-Sevcik coveragetion by measuring the CV of the $Fe(CN)_6^{3-/4-}$ couple (5 mM in 0.1 M PB), utilising a diffusion coefficient of 7.60×10^{-6} cm ^{2}/s. This afforded an electroactive surface area of 0.0056 cm^2, 1.47 times larger than the geometrical area, in good agreement with prior reports.[27] Electropolymerisation was carried out in an aqueous solution of 1 mL 98% aniline and 2 mL of 50% phytic acid (w/w in H_2O) with addition of 17 mL of MilliQ water by applying a current density of 10 µA/cm^2 for 5, 10, 20, 40 or 80 min. The films were rinsed with 0.1 M PB and then equilibrated in the same buffer for 10 min before further characterisation. Covalent immobilization of the receptor was carried out by exposure of the PANI-PA films to 2.5% glutaraldehyde (in PB) for 30 min, followed by rinsing with copious amounts of PB. The antibodies were then coupled to the activated interface by exposure to 5 µg/mL anti-CRP or 5 µg/mL anti-D-dimer for 30 min. After rinsing with 0.1 M 7.4 pH PB remaining active sites were deactivated with 10 mM ethanolamine in 0.1 M 7.4 pH PB for 30 min followed by rinsing with PB.

Protein assays: The sensor was equilibrated in PB for 30 min to obtain a stable baseline. Afterwards the sensor was exposed to increasing CRP concentration (0.25, 0.5, 1, 2, 4, 8, 16 µg/mL)) for 10 minutes followed by rinsing with copious amounts of PB. The redox capacitance was then measured in pure PB as described above.

RESULTS AND DISCUSSION

Phytic acid-doped polyaniline (PANI-PA) films on screen printed graphene nanoplate electrodes were generated by applying a controlled current density for specific and varied amounts of time (between 5 – 80 min, for details see experimental section). The FT-ATR-IR signatures of the so generated films include peaks at 1097, 1248 and 1719 cm^{-1} (Figure S1). The latter most likely arises from the phosphate groups of the phytic acid, indicating incorporation into the polymeric film. Phytic acid doping has been previously shown to endow the PANI films with higher conductivity in physiological pH and high hydrophilicity.[28,29] The latter is commonly associated with an increased resistance to non-specific adsorption and was assessed here by water contact angle measurements. As can be seen in Figure S2 the high water contact angle of the bare electrode (126°) is indicative of a hydrophobic interface which becomes gradually more hydrophilic with increasing PANI deposition (polymerization time). After 80 min a relatively hydrophilic film (43°) can be obtained.

The electrogenerated PANI-PA films were investigated by CV and EIS in 0.1 M PB, pH = 7.4 in the absence of any solution-phase redox probe. As can be seen in Figure 1a, the PANI films display a well-defined quasi-reversible redox couple at -0.16 V whose peak currents are, as expected, proportional to polymerization time (5 – 80 min). This is indicative of a continuous growth of the PANI film even at long polymerization times and enables good control over the PANI surface coverage and thus thickness. An increased film thickness also induces a larger peak separation, indicative of a predictably and progressively reduced electron transfer rate through thicker films. These general observations were also confirmed by impedance-derived capacitance measurements. In the capacitive Nyquist plots (Figure 1b) an increased redox-capacitance (C_r) at the "redox-in" potential (i.e. half-wave potential) can be resolved as the semi-circle diameter, which, again, is proportional to the polymerization time. This capacitance can also be obtained by fitting to an equivalent circuit (Figure S3), where R_s is the solution resistance and C_r the redox capacitance. Q_t and R_t are additional parameters that account for the non-ideal behavior of the porous polymer.[8,30,31] Importantly, C_r obtained via circuit fitting (utilized throughout herein) is almost identical to that obtained by graphical analysis and can further be utilized to quantify the surface coverage (Γ) of redox active aniline subunits ((1) eq. SI).[18] The hereby obtained molecular surface coverage (6-35 $nmolcm^{-2}$) is in a good agreement with that obtained by integration of the peak area in the CVs (deviations 2-20%, Figure S4, Table S1).

The same capacitive analyses outside of the window of PANI Faradaic activity (0.4 V), resolve capacitances that are much smaller (by at least one order of magnitude, Figure S5) than C_r measured at the redox potential. A direct analysis of capacitance at different potentials as described previously[32] confirms C_r to be directly correlated with the Faradaic activity of the film as resolved by SWV (Figure S6). Importantly, the baseline stability of C_r is excellent for all PANI-PA films (see inset of Figure 1b), being negligible after an initial brief stabilization.

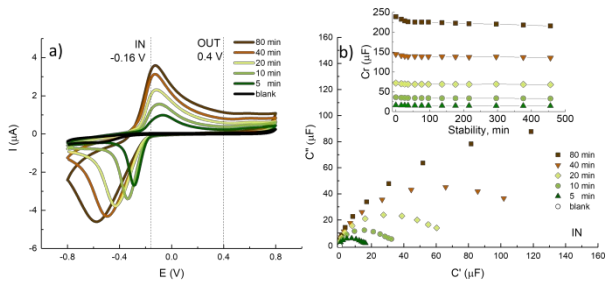

Figure 1. Electrochemical characterisation of PANI-PA films after different polymerization times (5-80 min) in 0.1 M PB, pH 7.4. a) CVs at scan rate of 100 mVs^{-1}. b) Capacitive Nyquist plots at redox IN potential (-0.16 V) where C_r can be resolved as the diameter of the semicircular region. The inset shows the temporal stability of C_r; after an initial signal decrease the baseline is stable within ≤2%.

Further analysis of the EIS data showed that the relaxation time constant (τ_r), which is associated with the Faradaic charging event, decreases with increasing film thickness (Figure S7, Table S2), indicative of slower electron transfer as similarly resolved by CV (vide supra).[32]

Subsequently, signal response/suppression of the PANI-PA films upon exposure to (several dilutions and 100 %) fetal bovine serum (FBS) was studied, an analysis which indirectly reports on fouling. Across all serum concentrations utilized the relative response (relative decrease in capacitance) was largest for the thinnest PANI film (5 min polymerisation), with thicker films being associated with a reduced signal suppression/fouling (Figure S8), an empirical observation in good agreement with enhanced interfacial hydration (as assessed by water contact angles). As expected, fouling is generally lower for more diluted FBS media.

The so generated film, with their tuneable redox capacitance and fouling profile, can be instilled with selective recognition

characteristics through the facile integration of receptors. As proof-of-concept, CRP, a clinically relevant biomarker for cardiovascular health, was chosen as the analyte and assayed in pure PB and 1% FBS. A selective CRP-receptive PANI-based interface was constructed by immobilization of anti-CRP *via* glutaraldehyde crosslinking of amine functionalities in the PANI film and the antibody. This induced a significant C_r response (75% signal change, from 32.7 ± 2.1 µF (PANI-10min) to 8.15 ± 0.32 µF (PANI/anti-CRP)) as shown in Figure S9, consistent with a large degree of anti-CRP recruitment. This was further confirmed by assessing the anti-CRP depletion from the immobilization solution using the Bradford assay, which revealed a total anti-CRP coverage of 909 ± 80 ng/cm^2 on PANI-10min. This receptor coverage is, as expected, larger than a monolayer coverage,[33] but interestingly also larger than that reported for other PANI films.[34]

Exposure of the receptive interface to CRP induces marked changes in its capacitive signatures which are easily resolved in capacitive Nyquist plots (a standard impedimetric analysis cannot report on these changes, Figure S10). The capacitive response of these anti-CRP modified PANI interfaces towards CRP in PB could be accurately described by a Langmuir-Freundlich adsorption isotherm (Figure 2a). Interestingly, the sensitivity of the sensor (as determined by the slope of the linear region in the calibration curve) decreases with increasing PANI coverage, as shown in Figure S11-d). We attribute this to an enhanced receptor-to-transducer ratio in the thinner films (the quantified antibody loading is constant within error, across different film thicknesses). If one assumes that only the outer periphery of the film is functionalized with the receptor, then thicker films will be associated with a greater proportion of redox charging entities more remote from the recognition process (and presumably less sensitive to it).

The optimal balance of sensitivity and fouling was observed for PANI-10min and this interface responds selectively to CRP in dilute serum with a response accurately described by a Langmuir-Freundlich adsorption isotherm (R^2 = 0.9995), with a K_d of 19 nM, n = 2.1 (indicative of a somewhat heterogeneous interface) and a maximum relative response of 38%. Over a linear range from 0.25 – 2 µg/mL this corresponds to a sensitivity of 24%/decade, significantly higher than that attainable for a previously reported Fc-SAM-based CRP sensor operating in pure buffer.[35] Importantly, these PANI-PA interfaces enable CRP detection across the whole clinical range, with a LOD of 0.5 µg/mL (4.5 nM).

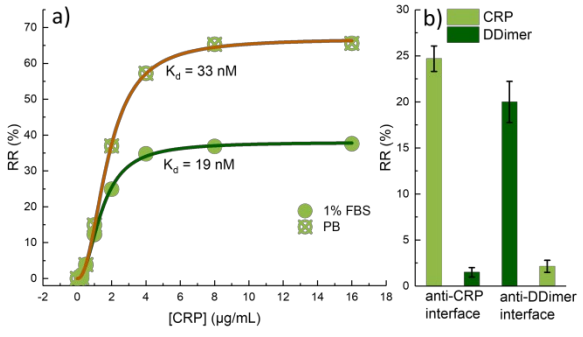

Figure 2. a) Relative response of PANI-10min/anti-CRP towards CRP in PB and in 1% of FBS in clinically relevant range. The data was fitted to a Langmuir-Freundlich isotherm. b) Relative response of anti-CRP or anti-D-dimer-modified PANI-10min after exposure to 2 µg/mL of CRP or D-dimer in 1% FBS. Error bars represent one standard deviation from independent measurements on different electrodes.

The interfacial specificity was additionally assessed by exposure of the anti-CRP/PANI-10min to spiked 1% FBS. Specifically, the most abundant proteins in human blood, fibrinogen, human serum albumin (HSA) and IgG were added at 100 µg/mL (a concentration that is both 50x higher than CRP and in the range expected for 1% serum). Importantly, the response was negligible (≤2%) in all of these controls (Figure S12). Assay selectivity was further confirmed by switching the IgG's between anti-CRP and anti-D-dimer (Figure 2b).

CONCLUSIONS

In summary, we report a novel redox capacitive biosensor based on a phytic acid-doped PANI polymer. This redox active support displayed excellent baseline stability (≤2% drift over 7 h after an initial stabilization over 30 min) and showed, without any further integration of antifouling components, a good resistance to non-specific protein adsorption. The redox charging features (scale and timeframe) are tunable through film thickness and enable a tuning of the sensitivity of the interface. The subsequent facile integration of a high antibody load generates interfaces of good target specificity. At optimal redox charging: receptor ratios a selective assaying of the cardiac biomarker CRP is possible across its entire clinically relevant range and down to 0.5 µg/mL. To the best of our knowledge this is the first report of a redox-active polymer in supporting reagentless redox capacitive biosensing. Importantly, the electropolymerisation assembly is readily translatable to any conductive surface (and any biomarker of interest).

ASSOCIATED CONTENT

Supporting Information

The Supporting Information is available free of charge on the ACS Publications website.

Additional experimental detail, surface characterisation and sensor performance.

AUTHOR INFORMATION

Corresponding Author

*E-mail: jason.davis@chem.ox.ac.uk. Phone: +44 1865 275914.

Author Contributions

The manuscript was written through contributions of all authors. / All authors have given approval to the final version of the manuscript.

Notes

The authors declare no competing financial interest.

ACKNOWLEDGMENT

We would like to acknowledge Dr. Kavita Pandey for scientific discussions and Dr. Amol V. Patil for providing a 3D antibody graphic. JJD and AB would like to thank to Innovate UK for funding.

REFERENCES

(1) Johnson, A.; Song, Q.; Ferrigno, P. K.; Bueno, P. R.; Davis, J. J.

Anal. Chem. **2012**, *84*, 6553−6560.
(2) Kausaite-minkstimiene, A.; Glumbokaite, L.; Ramanaviciene, A. *Microchem. J.* **2020**, *154*.
(3) Baradoke, A.; Juodkazyte, J.; Masilionis, I.; Selskis, A.; Pauliukaite, R.; Valiokas, R. *Microelectron. Eng.* **2019**, *208*, 39–46.
(4) Zucolotto, V.; Daghastanli, K. R. P.; Hayasaka, C. O.; Riul, A.; Ciancaglini, P.; Oliveira, O. N. *Anal. Chem.* **2007**, *79*, 2163–2167.
(5) Spain, E.; Gilgunn, S.; Sharma, S.; Adamson, K.; Carthy, E.; Kennedy, R. O.; Forster, R. J. *Biosens. Bioelectron.* **2016**, *77*, 759–766.
(6) Spain, E.; Carrara, S.; Adamson, K.; Ma, H.; Kennedy, R. O.; Cola, L. De; Forster, R. J.; Strasbourg, U. De. *ACS Omega* **2018**, *3*, 17116–17124.
(7) Forster, R. J.; Spain, E.; Adamson, K. *Curr. Option Electrochem.* **2017**, *3*, 63–67.
(8) Li, N.; Brahmendra, A.; Veloso, A. J.; Prashar, A.; Cheng, X. R.; Hung, V. W. S.; Guyard, C.; Terebiznik, M.; Kerman, K. *Anal. Chem.* **2012**, *84*, 3485–3488.
(9) Huang, Y.; Bell, M. C.; Suni, I. I. *Anal. Chem.* **2008**, *80*, 9157–9161.
(10) Wang, Y.; Li, C.; Li, X.; Li, Y.; Kraatz, H. B. *Anal. Chem.* **2008**, *80*, 2255–2260.
(11) Baradoke, A.; Jose, B.; Pauliukaite, R.; Forster, R. J. *Electrochim. Acta* **2019**, *306*, 299–306.
(12) Bogomolova, A.; Komarova, E.; Reber, K.; Gerasimov, T.; Yavuz, O.; Bhatt, S.; Aldissi, M. *Anal. Chem.* **2009**, *81*, 3944–3949.
(13) Kanyong, P.; Davis, J. J. *J. Electroanal. Chem.* **2019**, 113675.
(14) Xu, X.; Makaraviciute, A.; Kumar, S.; Wen, C.; Sjödin, M.; Abdurakhmanov, E.; Danielson, U. H.; Nyholm, L.; Zhang, Z. *Anal. Chem.* **2019**.
(15) Bueno, P. R. *Anal. Chem.* **2018**, *90*, 7095–7106.
(16) Fernandes, F. C. B.; Andrade, J. R.; Bueno, P. R. *Sensors Actuators B Chem.* **2019**, *291*, 493–501.
(17) Cecchetto, J.; Fernandes, F. C. B.; Lopes, R.; Bueno, P. R. *Biosens. Bioelectron.* **2017**, *87*, 949–956.
(18) Bueno, P. R.; Davis, J. J. *Anal. Chem.* **2014**, *86*, 1337–1341.
(19) Kang, D.; Ricci, F.; White, R. J.; Plaxco, K. W. *Anal. Chem.* **2016**, *88*, 10452–10458.
(20) Kang, D.; Zuo, X.; Yang, R.; Xia, F.; Plaxco, K. W.; White, R. J. *Anal. Chem.* **2009**, *81*, 9109–9113.
(21) Amarasiri, C.; Nguyen, T. B.; Nguyen, L. T.; Thu, V. T.; Thuy, N. T. M.; Dai Lam, T. *J. Electron. Mater.* **2017**, *46*, 5755–5763.
(22) Shoaie, N.; Forouzandeh, M.; Omidfar, K. *Microchim. Acta* **2018**, *185*.
(23) Zhu, F.; Lin, J.; Wu, Z. L.; Qu, S.; Yin, J.; Qian, J.; Zheng, Q. *ACS Appl. Mater. Interfaces* **2018**, *10*, 13685–13692.
(24) Erden, F.; Lai, S. C.; Chi, H.; Wang, F.; He, C. *ACS Omega* **2017**, *2*, 6506–6513.
(25) Baradoke, A.; Pastoriza-Santos, I.; González-Romero, E. *Electrochim. Acta* **2019**, *300*, 316–323.
(26) Deshmukh, M. A.; Celiesiute, R.; Ramanaviciene, A.; Shirsat, M. D.; Ramanavicius, A. *Electrochim. Acta* **2018**, *259*, 930–938.
(27) Favero, G.; Fusco, G.; Mazzei, F.; Tasca, F.; Antiochia, R. *Nanomaterials* **2015**, *5*, 1995–2006.
(28) Mawad, D.; Mansfield, C.; Lauto, A.; Perbellini, F.; Nelson, G. W.; Tonkin, J.; Bello, S. O.; Carrad, D. J.; Micolich, A. P.; Mahat, M. M.; et al. *Sci. Adv.* **2016**, *2*, e1601007.
(29) Pan, L.; Yu, G.; Zhai, D.; Lee, H. R.; Zhao, W.; Liu, N.; Wang, H.; Tee, B. C. K.; Shi, Y.; Cui, Y.; et al. *Proc. Natl. Acad. Sci. U. S. A.* **2012**, *109*, 9287–9292.
(30) Peng, W.; Aranda, C.; Bakr, O. M.; Garcia-Belmonte, G.; Bisquert, J.; Guerrero, A. *ACS Energy Lett.* **2018**, *3*, 1477–1481.
(31) Fournier-Wirth, C.; Coste, J.; Chebib, H.; Saikali, Y.; Vittori, O.; Errachid, A.; Cloarec, J.-P.; Martelet, C.; Jaffrezic-Renault, N. *Anal. Chem.* **2007**, *79*, 4879–4886.
(32) Bueno, P. R.; Davis, J. J. *Anal. Chem.* **2014**, *86*, 1997–2004.
(33) Geddes, N. J.; Paschinger, E. M.; Furlong, D. N.; Caruso, F.; Hoffmann, C. L.; Rabolt, J. F. *Thin Solid Films* **1995**, *260*, 192–199.
(34) Sai, V. V. R.; Mahajan, S.; Contractor, A. Q.; Mukherji, S. *Anal. Chem.* **2006**, *78*, 8368–8373.
(35) Piccoli, J.; Hein, R.; El-Sagheer, A. H.; Brown, T.; Cilli, E. M.; Bueno, P. R.; Davis, J. J. *Anal. Chem.* **2018**, *90*, 3005–3008.